# Accepted Manuscript


Morphological stability of an elastic tumor-host interface

E. Turian, K. Liu, J. Lowengrub, S. Li

PII: S0377-0427(18)30396-0
DOI: https://doi.org/10.1016/j.cam.2018.06.044
Reference: CAM 11774

To appear in: *Journal of Computational and Applied Mathematics*

Received date : 7 February 2018
Revised date : 23 May 2018

Please cite this article as: E. Turian, K. Liu, J. Lowengrub, S. Li, Morphological stability of an elastic tumor-host interface, *Journal of Computational and Applied Mathematics* (2018), https://doi.org/10.1016/j.cam.2018.06.044

# Morphological stability of an elastic tumor-host interface

E. Turian[a,c], K. Liu[b], J. Lowengrub[b], S. Li[a,*]

[a] *Department of Mathematics, IIT, Chicago, IL, 60616*
[b] *Department of Mathematics, University of California at Irvine, CA, 92617*
[c] *Present Address: Department of Mathematics, Northeastern Illinois University, Chicago, IL 60625*

**Abstract**

The ability of tumors to metastasize is preceded by morphological instabilities such as chains or fingers that invade the host environment. Therefore, parameters that control the morphology of the tumor may also contribute to its invasive ability. Previous analyses on morphological changes were performed using surface energy of the tumor-host interface. In an effort to understand the role the interface stiffness plays on tumor evolution, here we model the tumor-host interface as an elastic membrane governed by the Helfrich bending energy. Using an energy variation approach, we derive a modified Laplace-Young condition for the stress jump across the interface in the Stokes equation. We then perform a linear stability analysis and investigate how physical parameters such as viscosity, bending rigidity, and apoptosis affect the morphological instability. Results show that increased bending rigidity versus mitosis rate contributes to a more stable morphological tumor behavior. On the other hand, increasing tumor viscosity or apoptosis may lead to invasive fingering morphologies. Comparison with experimental data on glioblastoma spheroids shows good agreement especially for tumors with high adhesion and low proliferation.

*Keywords:* morphology, bending rigidity, mitosis, apoptosis, elastic energy, linear stability,
*2010 MSC:* 00-01, 99-00

## 1. Introduction

Advances in cancer research are hampered, to some extent, by the lack of theoretical models capable of describing the tumor evolution in vitro or in vivo. In turn, this gap leads to excessive and expensive biological experiments of limited utility (e.g. Byrne [1]). Understanding tumor

*Corresponding author
*Email address:* sli@math.iit.edu (S. Li )

morphology through the development of theoretical models has the potential to provide insights into critical parameters that control the dynamics of tumor growth [2, 3].

In order to understand the bio-mechanical properties of the tumor and its host environment, models based on fluid mechanics were employed. The Darcy model was used by Greenspan [4], Byrne and Chaplain [5], Friedman and Reitich [6] and Cristini *et al.* [7] among others. The Stokes model was considered by Friedman and Hu [8], and Friedman and Reitich [9]. Darcy & Stokes models were also considered by Franks and King [10, 11, 12]. Friedman and Hu [13] acknowledged that tumors grown in vitro tend to develop a more spherical shape, however, in vivo tumors usually develop a variety of shapes due to accelerated formations of protrusions. Furthermore, the morphological stability is characterized using an aggressiveness parameter defined by the ratio of the proliferation rate and the cell-to-cell adhesiveness, and it is shown that spherical tumors become unstable before the aggressiveness parameter reaches its bifurcation point (at least for certain unperturbed radial values). Recently, Pham *et al.* [14] evaluated the morphological stability of growing tumors using three continuum models (Darcy law, Stokes law, and a combined Darcy-Stokes law). Their analysis suggests that the Stokes model is more consistent with experimental findings for in vitro spheroids.

Tumor tissues may have different mechanical properties compared to their surroundings. Examples include breast, lung, head & neck, and brain metastasis. In particular, breast cancer can be found simply by physical examinations, as the cancerous lump is stiffer than the healthy host [15]. For this type of cancer, tumor elasticity can be associated with prognostic histologic features (size, tumor histological type, grade, or lymph node status) [16], or metastasis [17]. The study conducted by Fenner at al. [17] suggests that increased tumor stiffness contributes to smaller local recurrence and less extensive metastases than softer elastic tumors. Also, it has been reported that changes in stiffness of Extra-Cellular Matrix (ECM) contribute to tumor growth and metastasis [18], and can lead to increased mitosis and migration [15].

In this work we develop a model to address the difference of mechanical properties between the tumor and its host. We model the tumor-host interface as an elastic membrane with bending rigidity $\nu_0$ and consider the elastic Helfrich bending energy instead of the surface energy of a fluid-fluid interface. Using an energy variation approach, we derive a modified stress jump boundary condition for the Stokes equation. Moreover, our study introduces a new parameter $\mathbb{S}$ characterizing the relative ratio of cell mitosis rate to membrane rigidity. We hope our studies can shed light on the elastic behavior of the tumor-host interface and help physicians to design more effective cancer-

therapies. Note that the bending energy has been considered in other physical and biophysical contexts, e.g. [19, 20, 21, 22, 23].

Our purpose is two-fold. Firstly, we aim to establish a mathematical framework for studying the morphological growth stages of tumor spheroids in a two-phase Stokes flow in 2D. We model the tumor and its host as viscous fluids and use the Stokes equation to describe the tumor dynamics. We assume that the tumor cell population is homogeneous, and pressure acts as an expansion force due to cell proliferation. The externally supplied cell substrates contribute to tumor growth and regulate processes such as apoptosis and mitosis. After nondimensionalizing and redefining the entire system of equations (derived in section 3), we seek a linear solution to the nutrient concentration, pressure and the velocity field using a perturbed circular interface.

Secondly, using a parameter–the relative time variation of the shape factor (defined later in Sec.2), we perform a sensitivity analysis to investigate the key parameters, including apoptosis, the effect of blood (also found in [7]), the ratio of the exterior to interior viscosities (also found in [24]), the membrane's bending rigidity, and the ratio of mitosis rate to rigidity. Linear stability analysis suggests that all the parameters listed above influence tumor morphology.

We found that during the avascular stage, larger apoptosis values produce increased morphological instabilities. Meanwhile, the mitosis rate to rigidity is the most influential parameter. As expected, larger bending rigidity leads to higher morphological stability. For most of the parameter values in this study, we find that larger radial tumors tend to maintain their level of stability. Our model is consistent with experimental results in the case of high adhesion and low proliferation and low cell adhesion and high proliferation.

The rest of the paper is organized as follows. In section 2, we present the Governing Equations for the growth of the tumor and the ones representing the host environment. In section 3, we nondimensionalize the entire system and reformulate the interior model to a divergence free Stokes model. In section 4, we obtain the linear solutions of the newly created systems of equations. In section 5, we analyze tumor's morphology during different stages of avascular and vascular growth. Section 6 evaluates our findings based on our model against observations from experiments with in vitro tumor growth. Finally, in section 7, we draw our conclusions.

## 2. Mathematical Model

Here we consider a domain $\Omega$ consisting of a tumor region $\Omega_-(t)$ and a healthy surroundings tissue $\Omega_+(t)$. In between, there is a sharp interface $\Sigma(t)$ separating the two regions, as shown in Figure 1. The " $-$ " and " $+$ " subscript notations indicate the interior tumor and exterior host, respectively. Our work considers the following elastic energy

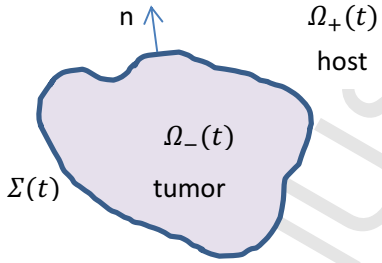


Figure 1: Tumor and its exterior host environment.

$$E = \frac{1}{2}\int_{\Sigma} \nu_0 \mathcal{K}^2 ds, \tag{1}$$

where $\mathcal{K}$ is the local curvature, $\nu_0$ is the constant bending rigidity factor, $s$ is the arc length.

The governing equations for the growth of a non-necrotic tumor can be written as follows,
(A) Incompressibility in $\Omega_-(t)$ and $\Omega_+(t)$:

$$\nabla \cdot \mathbf{v}_- = \lambda_P \quad (\text{in} \quad \Omega_-(t)), \tag{2}$$

where $\mathbf{v}_-$ is the fluid velocity in tumor region, and $\lambda_P$ is the net cell-proliferation rate given by

$$\lambda_P = b\sigma - \lambda_A, \tag{3}$$

where $\sigma$ is the concentration of the cell substrates (e.g. oxygen, nutrients, and growth factors), $b$ the blood factor and $\lambda_A$ the rate of apoptosis. Assuming that both $b$ and $\lambda_A$ are uniform, and no proliferation in the host,

$$\nabla \cdot \mathbf{v}_+ = 0 \quad (\text{in} \quad \Omega_+(t)), \tag{4}$$

where $\mathbf{v}_+$ is the host tissue velocity.

(B) Diffusion in $\Omega_-(t)$ and $\Omega_+(t)$:

$$\sigma_t = \nabla \cdot (\mathbb{D}\nabla\sigma) + \Gamma \qquad (\text{in} \quad \Omega_-(\text{t})), \tag{5}$$

where $\mathbb{D}$ represents the diffusion coefficient and $\Gamma$ the rate at which cell substrates are brought into $\Omega_-$. The substrates are supplied by a vasculature at a rate $\Gamma_B$:

$$\Gamma_B = -\lambda_B(\sigma - \sigma_B), \tag{6}$$

where $\lambda_B$ is the transfer rate between the blood and the tissue, and $\sigma_B$ is the substrate concentration, which is uniform in the blood. The net consumption rate $\Gamma$ is given by

$$\Gamma = -\lambda_\sigma \sigma + \Gamma_B, \tag{7}$$

where $\lambda_\sigma$ is the uptake rate. We assume that the cell substrate concentration $\sigma$ is constant in $\Omega_+(t)$:

$$\sigma = \sigma_\infty. \tag{8}$$

(C) The Stokes equation in $\Omega_-(t)$ and $\Omega_+(t)$:

$$\nabla \cdot \ \mathbf{T}_\pm = 0, \tag{9}$$

where $\mathbf{T}_\pm$ are stress tensors for interior tumor (-) and exterior host (+),

$$\mathbf{T}_\pm = \mu_\pm(\nabla\mathbf{v}_\pm + (\nabla\mathbf{v}_\pm)^T) + \bar{\mu}_\pm(\nabla\cdot\mathbf{v}_\pm)\mathbf{I} - p_\pm\mathbf{I}, \tag{10}$$

where parameters $\mu_\pm$ and $\bar{\mu}_\pm$ are the viscosity coefficients, and $p_\pm$ are pressures. Note that the stress tensors take into account the rate of strain, dilatation and pressure.

(D) Across the interface $\Sigma(t)$:

$$\sigma_\Sigma = \sigma_\infty, \tag{11}$$

$$[\mathbf{v}] = \mathbf{v}_+ - \mathbf{v}_- = 0. \tag{12}$$

The interface $\Sigma(t)$ is sharp and treated here as a one-dimensional curve with zero-thickness.

(E) Boundary condition:

$$[\mathbf{Tn}] = -\nu_0 \left(\frac{1}{2}\mathcal{K}^3 + \mathcal{K}_{ss}\right)\mathbf{n}, \tag{13}$$

which is the stress jump across the interface [19] given by the vanishing of the first variation of Eq. (1). Here $(\cdot)_s$ represents derivative with respect to the arclength $s$, and $\mathbf{n}$ is the outward unit normal to the interface.

## 3. Non-dimensionalization and Model Reformulation

The dimensional variables are rescaled by their characteristic values yielding the following non-dimensional parameters:

$$\mathbf{x}' = \frac{\mathbf{x}}{L}, \quad t' = \lambda_t t, \quad \sigma' = \frac{\sigma}{\sigma_\infty}, \quad p'_\pm = \frac{p_\pm}{\bar{P}_-}, \quad \mathbf{T}'_\pm = \frac{\mathbf{T}_\pm}{\bar{T}_-}, \quad \mathcal{K}' = L\mathcal{K}, \quad s' = \frac{s}{L}, \tag{14}$$

where L, $\lambda_t$ and $\sigma_\infty$ are scales used for length, time and nutrient concentration, respectively. Also, $\bar{P}_-=\bar{T}_-=\mu_-\lambda_M$. The effective mitosis rate is considered to be proportional to the cell substrate level at the interface, i.e., $\lambda_M = b\sigma_\infty$. The non-dimensional velocity reads

$$\mathbf{v}'_\pm = \frac{\mathbf{v}_\pm}{\lambda_t L}. \tag{15}$$

From Eq. (2), the intrinsic time scale is obtained as

$$\lambda_t = \lambda_M. \tag{16}$$

And by Eq. (5) we can obtain the following intrinsic length scale

$$L = \sqrt{\frac{\mathbb{D}}{\lambda_B + \lambda_\sigma}}. \tag{17}$$

The nondimensionalization process leads to the following nondimensional parameters:

- The relative effect of vascularization:

$$\mathbb{B} = \frac{\sigma_B}{\sigma_\infty}\frac{\lambda_B}{\lambda_B + \lambda_\sigma}. \tag{18}$$

- The relative ratio of cell apoptosis to mitosis rates:

$$\mathbb{A} = \frac{\lambda_A}{\lambda_M} - \mathbb{B}. \tag{19}$$

- The relative ratio of membrane rigidity to cell mitosis rate:

$$\mathbb{S}^{-1} = \frac{\nu_0}{\mu_-\lambda_M L^3}. \tag{20}$$

- The ratio between two interior viscosity:

$$\bar{\lambda} = \frac{\bar{\mu}_-}{\mu_-}. \tag{21}$$

- The ratio between the exterior and interior viscosities:

$$\lambda = \frac{\mu_+}{\mu_-}. \tag{22}$$

By introducing a redefined concentration

$$\sigma' = \mathbb{B} + (1 - \mathbb{B})\bar{\sigma} \tag{23}$$

and dropping the bars and the primes, we obtain the following non-dimensional system for the two-sided tumor model.

(1) Equations for the tumor region, $\Omega_-(t)$:

$$\begin{cases} \text{Incompressibility } \nabla \cdot \mathbf{v}_- = (1 - \mathbb{B})\sigma - \mathbb{A}, \\ \text{Stokes equation } \nabla \cdot \mathbf{T}_- = 0, \\ \text{Nutrient equation } \Delta\sigma = \sigma, \end{cases} \tag{24}$$

where $\mathbf{T}_- = \nabla\mathbf{v}_- + (\nabla\mathbf{v}_-)^T - \bar{p}_-\mathbf{I}$ and $\bar{p}_- = p_- - \bar{\lambda}\nabla \cdot \mathbf{v}_-$ is a modified pressure.

We arrived at the simplified version of the nutrient equation presented in (24) by using the assumption that the nutrient diffusion happens much faster than mitosis, i.e. $(\lambda_M L^2/\mathbb{D}) \ll 1$.

(2) Equations for the host environment, $\Omega_+(t)$:

$$\begin{cases} \text{Incompressibility } \nabla \cdot \mathbf{v}_+ = 0, \\ \text{Stokes equation } \nabla \cdot \mathbf{T}_+ = 0, \\ \text{Nutrient equation } \sigma = 1, \end{cases} \tag{25}$$

where $\mathbf{T}_+ = \lambda(\nabla\mathbf{v}_+ + (\nabla\mathbf{v}_+)^T) - p_+\mathbf{I}$.

(3) Boundary conditions at the interface $\Sigma(t)$:

$$\begin{cases} \sigma = 1, \\ \mathbf{v}_+ - \mathbf{v}_- = 0, \\ \mathbf{T}_+\mathbf{n} - \mathbf{T}_-\mathbf{n} = -\mathbb{S}^{-1}\left(\frac{1}{2}\mathcal{K}^3 + \mathcal{K}_{ss}\right)\mathbf{n}. \end{cases} \tag{26}$$

Next, the equations related to the tumor region are reformulated to a standard Stokes divergence-free model, by redefining the velocity as:

$$\mathbf{u}_- = \mathbf{v}_- - (1-\mathbb{B})\nabla\sigma + \frac{\mathbb{A}\mathbf{x}}{d}, \tag{27}$$

where $d$ is the spatial dimension ($d = 2$ for our two dimensional model). As such, the interior redefined tumor model becomes:

(1') The redefined interior model equations:

$$\begin{cases} \mathsf{Incompressibility}\ \ \nabla\cdot\mathbf{u}_- = 0, \\ \mathsf{Stokes\ \ equation}\ \ \Delta\mathbf{u}_- = \nabla\tilde{p}_-, \\ \mathsf{Nutrient\ \ equation}\ \ \Delta\sigma = \sigma. \end{cases} \tag{28}$$

where $\tilde{p}_-$ is the renamed interior pressure $\tilde{p}_- = \bar{p}_- - \nabla\cdot\mathbf{v}_- - (1-\mathbb{B})\sigma$. Meanwhile, the boundary conditions become:

(3') The reformulated boundary conditions:

$$\begin{cases} \sigma = 1, \\ \mathbf{v}_+(\mathbf{x})|_\Sigma - \mathbf{u}_-(\mathbf{x})|_\Sigma = (1-\mathbb{B})\nabla\sigma|_\Sigma - \frac{\mathbb{A}\mathbf{x}_\Sigma}{2}, \\ \mathbf{T}_+\mathbf{n} - \mathbf{T}_-^u\mathbf{n} = -\mathbb{S}^{-1}\left(\frac{1}{2}\mathcal{K}^3 + \mathcal{K}_{ss}\right)\mathbf{n} + 2(1-\mathbb{B})\nabla\nabla\sigma\mathbf{n} - 2(1-B)\sigma\mathbf{n} - \frac{\mathbb{A}}{d}(2-d)\mathbf{n}, \end{cases} \tag{29}$$

where $T_-^u = \nabla u_- + (\nabla u_-)^T - \tilde{p}_- I$.

## 4. Linear Solutions

We assume the interface $\Sigma(t)$ is a perturbed circle

$$r(t,\theta) = R(t) + \delta(t)e^{il\theta}, \tag{30}$$

where $R(t)$ is the radius of the underlying circle, $l$ is the polar wave number, $\theta$ the polar angle, and $\delta(t)$ the size of the perturbation as shown in Figure 2.

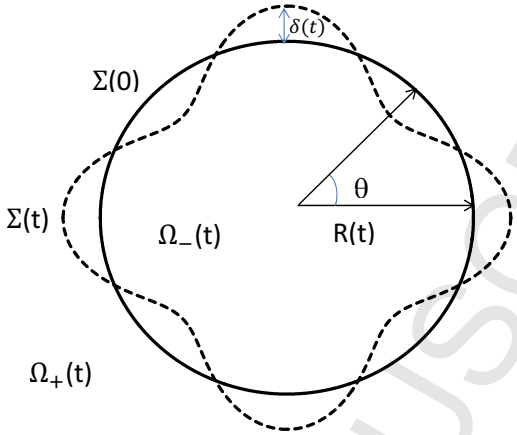


Figure 2: The perturbed tumor with mode $l = 4$.

The radial solutions can then be written as:

$$\begin{cases} \tilde{p}_-^{(0)}(r) = A_{\tilde{p}}, \\ u_-^{(0)}(r) = 0, \\ \sigma_-^{(0)}(r) = \frac{I_0(r)}{I_0(R)}, \end{cases} \quad \text{in } \Omega_-(t) \tag{31}$$

where $I_k(r)$ is the $k$-th modified Bessel function of the first kind and $A_{\tilde{p}}$ is a constant, and

$$\begin{cases} p_+^{(0)}(r) = A_p, \\ v_+^{(0)}(r) = \frac{A_v}{r}, \\ \sigma_+^{(0)}(r) = 1, \end{cases} \quad \text{in } \Omega_+(t) \tag{32}$$

where $A_p$ and $A_v$ are also constants.

We next perform a linear stability analysis using the reformulated, non-dimensional system in two dimensions. On the perturbed interface, the linear solutions for the systems described by (1'),

(2) and (3') take the following form:

$$\begin{cases} \mathbf{u}_-(r,\theta) = u_-^{(0)}(r)\hat{\mathbf{r}} + \delta u_{-r}^{(1)}(r,\theta)\hat{\mathbf{r}} + \delta u_{-\theta}^{(1)}(r,\theta)\hat{\boldsymbol{\theta}}, \\ \tilde{p}_-(r,\theta) = \tilde{p}_-^{(0)}(r) + \delta\tilde{p}_-^{(1)}(r,\theta), \\ \sigma_-(r,\theta) = \sigma_-^{(0)}(r) + \delta\sigma_-^{(1)}(r,\theta). \end{cases} \tag{33}$$

where $\hat{\mathbf{r}}$, $\hat{\boldsymbol{\theta}}$ are the unit base vectors for polar coordinates, and

$$\begin{cases} \mathbf{v}_+(r,\theta) = v_+^{(0)}(r)\hat{\mathbf{r}} + \delta v_{+r}^{(1)}(r,\theta)\hat{\mathbf{r}} + \delta v_{+\theta}^{(1)}(r,\theta)\hat{\boldsymbol{\theta}}, \\ p_+(r,\theta) = p_+^{(0)}(r) + \delta p_+^{(1)}(r,\theta), \\ \sigma_+(r) = 1. \end{cases} \tag{34}$$

I) Equations and linear solutions for the interior tumor $\Omega_-(t)$:

By applying Eq. (33) to system (1'), a new system can be formed representing the perturbed portion of the interior system:

$$\begin{cases} \mathsf{Incompressibility}\ \ \nabla\cdot\mathbf{u}_-^{(1)} = 0, \\ \mathsf{Stokes\ \ equation}\ \ \Delta\mathbf{u}_-^{(1)} = \nabla\tilde{p}_-^{(1)}, \\ \mathsf{Nutrient\ \ equation}\ \ \Delta\sigma^{(1)} = \sigma^{(1)}. \end{cases} \tag{35}$$

The linear solutions for the Eq. (35) can be shown to take the following form:

$$\begin{cases} \tilde{p}_-^{(1)} = B_{pt} r^l e^{il\theta}, \\ u_{-r}^{(1)} = (\frac{B_{pt} l r^{l+1}}{4(l+1)} + l B_u r^{l-1}) e^{il\theta}, \\ u_{-\theta}^{(1)} = (\frac{B_{pt}(l+2) r^{l+1}}{4l(l+1)} + B_u r^{l-1})\partial_\theta e^{il\theta}, \\ \sigma_-^{(1)} = A_\sigma J_l(ir) e^{il\theta}. \end{cases} \tag{36}$$

where $B_{pt}$ and $B_u$ are coefficients to be determined, $A_\sigma = -\frac{I_1(R)}{I_0(R)}\frac{1}{J_l(iR)}$, and $J_k(r)$ is the $k$-th order Bessel function of the first kind.

Therefore, we write the linear solutions of the equations represented by system (1'):

$$\begin{cases} \tilde{p}_- = A_{\tilde{p}} + \delta B_{pt} r^l e^{il\theta}, \\ \mathbf{u}_- = \delta\left((\frac{B_{pt} l r^{l+1}}{4(l+1)} + l B_u r^{l-1}) e^{il\theta}\hat{\mathbf{r}} + (\frac{B_{pt}(l+2) r^{l+1}}{4l(l+1)} + B_u r^{l-1})\partial_\theta e^{il\theta}\hat{\boldsymbol{\theta}}\right), \\ \sigma_- = \frac{I_0(r)}{I_0(R)} + A_\sigma J_l(ir) e^{il\theta}\delta. \end{cases} \tag{37}$$

II) Equations and linear solutions for the host region $\Omega_+(t)$:

The perturbed portion of the system represented by the system (2), for the exterior model, can similarly be grouped as follow:

$$\begin{cases} \text{Incompressibility } \nabla \cdot \mathbf{v}_+^{(1)} = 0, \\ \text{Stokes equation } \Delta \mathbf{v}_+^{(1)} = \nabla p_+^{(1)}, \\ \text{Nutrient equation } \sigma^{(1)} = 0. \end{cases} \tag{38}$$

Similarly, the linear solutions to Eq. (38) are given by:

$$\begin{cases} p_+^{(1)} = B_p r^{-l} e^{il\theta}, \\ v_{+r}^{(1)} = (\frac{B_p l r^{1-l}}{4(l-1)} - B_v l r^{-1-l}) e^{il\theta}, \\ v_{+\theta}^{(1)} = (\frac{-B_p(-2+l) r^{1-l}}{4(l-1)l} + B_v r^{-1-l}) \partial_\theta e^{il\theta}, \end{cases} \tag{39}$$

where $B_p$ and $B_v$ are coefficients to be determined. Using Eqs. (32) and (39), the linear solutions for system (2) take the following form

$$\begin{cases} p_+ = A_p + \delta B_p r^{-l} e^{il\theta}, \\ \mathbf{v}_+ = \frac{A_v}{r} \hat{\mathbf{r}} + \delta \left( \frac{B_p l r^{1-l}}{4(l-1)} - B_v l r^{-1-l} \right) e^{il\theta} \hat{\mathbf{r}} + \delta \left( \frac{-B_p(-2+l) r^{1-l}}{4(l-1)l} + B_v r^{-1-l}) \right) \partial_\theta e^{il\theta} \hat{\boldsymbol{\theta}}, \\ \sigma_+ = 1. \end{cases} \tag{40}$$

## 5. Morphological Stability Analysis

The continuous change in tumor morphology is analyzed by comparing the normal component of the velocity field in the following two forms:

$$V = \frac{dR(t)}{dt} + \frac{d\delta(t)}{dt} e^{il\theta}, \tag{41}$$

and

$$V = \mathbf{v}_+ \cdot \mathbf{n} = v_+^{(0)}(R) + \delta (\frac{dv_+^{(0)}}{dr}|_{r=R}) e^{il\theta} + \delta v_{+r}^{(1)}(R), \tag{42}$$

where the unit normal to the surface $\mathbf{n} = \mathbf{r} - (1/r)il\delta e^{il\theta}\boldsymbol{\theta}$.

From the velocity continuity condition (29) and Eqs. (41) and (42), the rate at which the circular radius is evolving is found to take the following form:

$$\frac{dR}{dt} = (1-B)\frac{I_1(R)}{I_0(R)} - \frac{\mathbb{A}R}{2}. \tag{43}$$

In Figure 3 we show the rate of change of a radial tumor with respect to $R$ for different $\mathbb{A}$ values. The plot suggests that for $\mathbb{A} = 0$ (no apoptosis), radial tumors exhibit growth only. For $0 < \mathbb{A} < 1$, radial tumors grow to a stationary state $\frac{dR}{dt} = 0$ according to the value of $\mathbb{A}$.

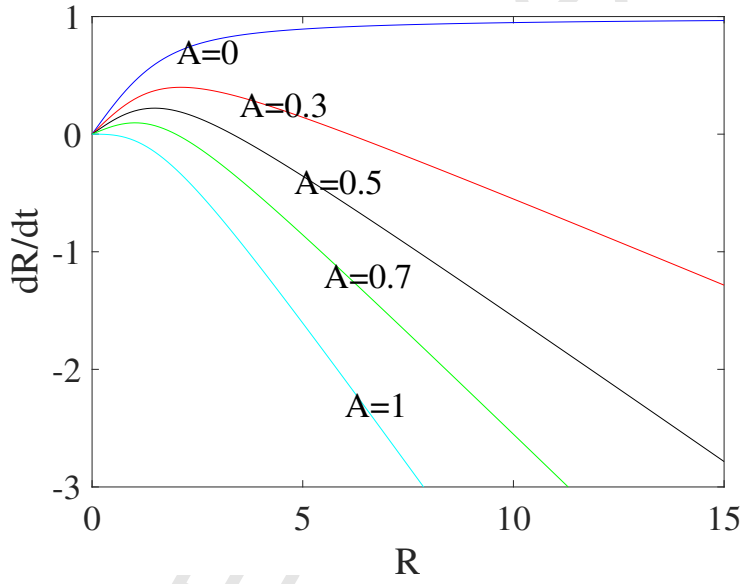


Figure 3: Growth rate from Eq. (43) for the radially symmetric tumor as a function of $R$. $\mathbb{B} = 0$.

By equating the corresponding coefficients of $\delta$ provided by Eqs. (41) and (42), we obtain the growth rate of the perturbation:

$$c = \left(\frac{\delta}{R}\right)^{-1}\frac{d(\frac{\delta}{R})}{dt} = \mathbb{A}\left(1 - \frac{1}{\lambda+1}\right) + \frac{l\mathbb{S}^{-1}}{4R^3}\left(\frac{3}{2} - l^2\right) + \frac{1-B}{1+\lambda}\left(1 - \frac{I_1(R)I_{l+1}(R)}{I_0(R)I_l(R)}\right) - (1-B)\frac{2}{R}\frac{I_1(R)}{I_0(R)}, \tag{44}$$

where $c$ represents the relative time variation of the shape factor $(\frac{\delta}{R})$, and describes the tumor morphological stability. Note that here we focus on the normal contribution of the term $\nabla\nabla\sigma$ in the stress jump.

It is known that the time variation of the shape factor can be categorized as positive, zero, or negative values, which correspond to unstable, self-similar, or stable growths, respectively. Equation (44) suggests that increased $\mathbb{A}$ values lead to increased morphological instability, which is consistent with previous findings [24]. It can also be seen from equation (44) that greater bending rigidity value leads to increased morphological stability.

### *5.1. Tumor's morphological stability during the avascular stage* ($\mathbb{B} = 0$)

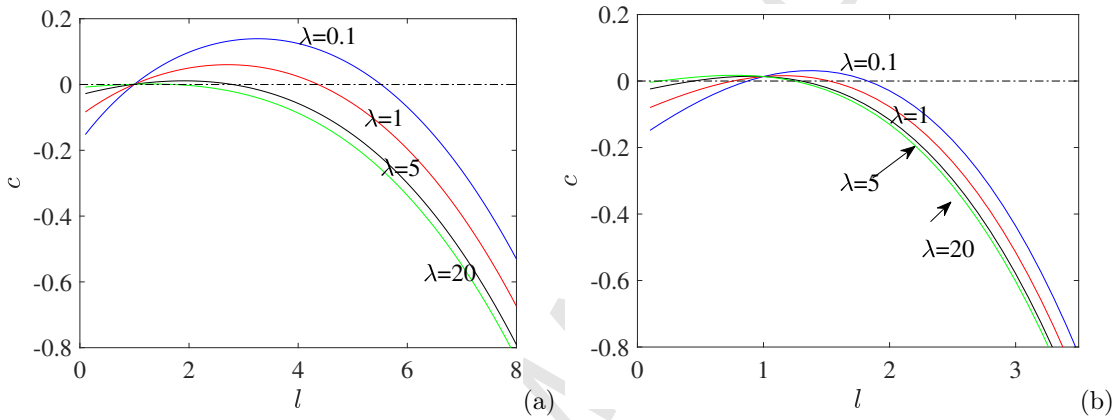


Figure 4: Relative change of the shape factor $c$ as a function of $l$ for different $\lambda$ values; $\mathbb{B} = 0$, $\mathbb{A} = 0.5$, and $\mathbb{S}^{-1} = 1/4$ (a) versus $\mathbb{S}^{-1} = 4$ (b).

Considering $\mathbb{A} = 0.5$, the right side of Eq. (43) equals to 0 (steady-state) when $R = 3.32585$. For these parameter values, we plot $c$ against $l$ in Figure 4 for $\mathbb{S}^{-1} = 1/4$ and $\mathbb{S}^{-1} = 4$. Recall $\mathbb{S}^{-1}$ is defined as the bending rigidity over mitosis rate. It can be seen from the two plots that $\mathbb{S}^{-1}$ decreases the growth rate of the perturbation, suggesting that increased bending rigidity and viscosity ratio contributes to a more stable behavior. Note that Figure 4 shows continuous curves of $l$ in order to provide all the values that illustrate clearly the boundary between the stable and unstable regions.

In Figure 5, we plot the evolution of the shape factor $c$ against the tumor size $R$. For simplicity, we set $\mathbb{S}^{-1} = 1/4$ for these calculations. Similar results hold for other $\mathbb{S}^{-1}$ values (not shown). From Eq. (43), we know $R$ will grow unbounded if the apoptosis parameter $\mathbb{A} = 0$. Interestingly, as $R$ increases, we observe the growth rate $c \to 0$ asymptotically in Figure 5 [a], i.e. the linear theory predicts that the morphologies of growing tumors tend to limiting shapes that evolve self-similarly.

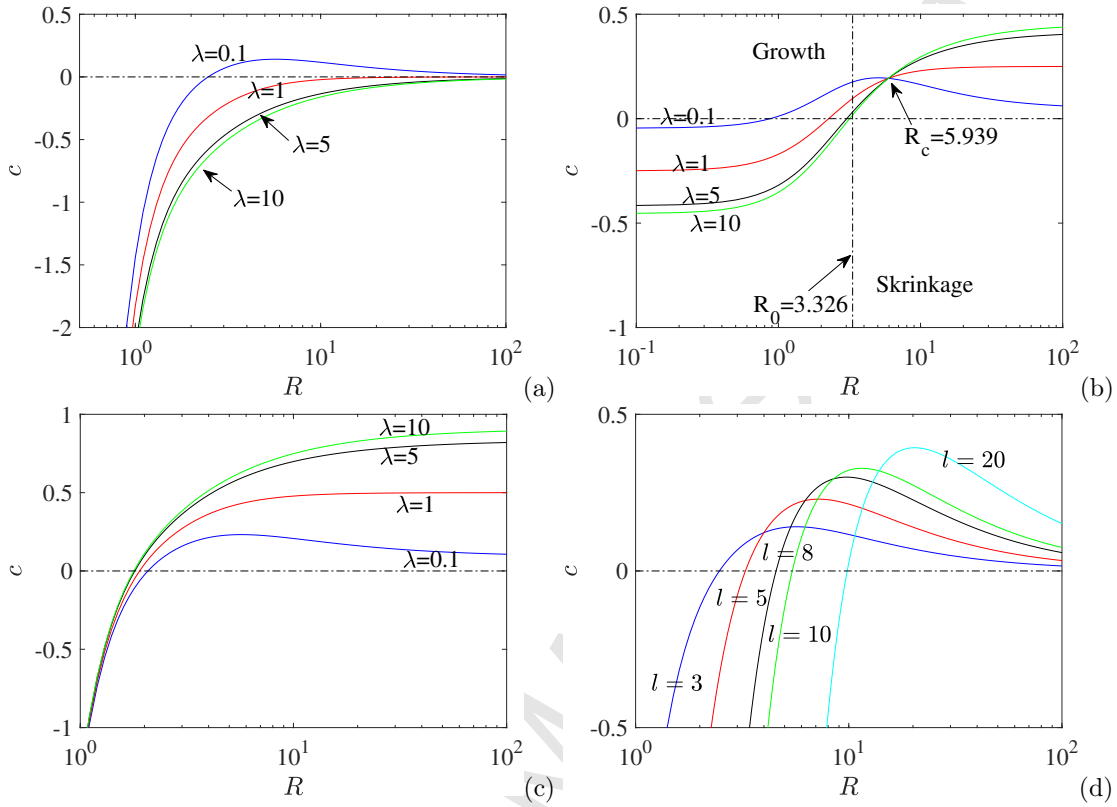


Figure 5: Relative change of the shape factor $c$ as a function of $R$ with $\mathbb{S}^{-1} = 1/4$. [a] $\mathbb{A} = 0$ and $l = 3$; [b] $\mathbb{A} = 0.5$ and $l = 3$; [c] $\mathbb{A} = 1.0$ and $l = 3$; [d] $\mathbb{A} = 0$ and $\lambda = 0.1$.

We next set $\mathbb{A} = 0.5$ in Figure 5 [b]. From Eq. (43), we know there exist both growth (when the size of the tumor $R < 3.326$) and shrinkage (when the size of the tumor $R > 3.326$). In particular, there exists a critical tumor size at $R = 5.939$ such that the growth rate of the shape factor $c$ is independent of the viscosity ratio. That is at this point, the tumor shrinks at the same rate. If we continue to increase the value of $\mathbb{A} = 1.0$ as shown in Figure 5 [c], there exists shrinkage only from Eq. (43). However, for large tumor size with $c > 0$, we have shrinking instability. That is the perturbation actually grows while the tumor size is shrinking. This might explain the formation of branched fingering structures that could occasionally take place after the treatment of chemo- or radiotherapy. In Figure 5 [d], we demonstrate how the evolution of shape factor $c$ depends on the perturbation mode $l$ using $\lambda = 0.1$ and $\mathbb{A} = 0$. Similar to the case $l = 3$, the growth rate $c \to 0$ asymptotically as $R \to \infty$.

*5.2. Tumor's morphological stability during the vascular stage* ($\mathbb{B} \neq 0$)

Next, we investigate the changes in $c$ for different vascular stages. In Figure 6, we plot the evolution of the shape factor, $c$ as a function of tumor size $R$. When $0 < \mathbb{B} < 1$, the growth rate of $R$ exhibits similar behavior as shown in Figure 3 governed by Eq. (43). We first set $\mathbb{B} = 0.5$ and $\mathbb{A} = 0$ (the mitosis rate is twice the rate of apoptosis), i.e. we study an ever-growing tumor in Figure 6[a]. Similar to what we obtained in Figure 5 [a], we observe linear self-similar growth, and the growth rate $c \to 0$ asymptotically as $R \to \infty$. Figure 6[a] also suggests that the morphology is becoming slightly more stable with increasing $\lambda$ values (host viscosity becoming larger than the one of the tumor). Moreover, when $\mathbb{B} = 1$ and $\mathbb{A} = 0$, we have $\frac{dR}{dt} = 0$, and $c = \frac{l\mathbb{S}^{-1}}{4R^3}\left(\frac{3}{2} - l^2\right)$, the tumor displays a stable morphology for small radial values ($c < 0$) and self similar evolution for larger ones ($c \approx 0$), independent of viscosity, as shown in Figure 6[b].

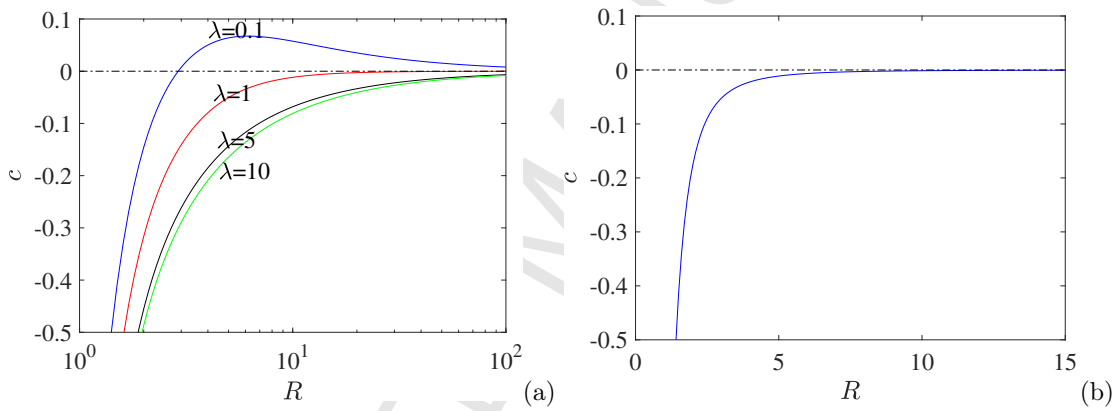


Figure 6: Relative change of the shape factor $c$ as a function or $R$ for different $\lambda$ values; $\mathbb{A} = 0$, $l = 3$, $\mathbb{S}^{-1} = 1/4$ and $\mathbb{B} = 0.5$ (a) vs. $\mathbb{B} = 1$ (b).

## 6. Model Assessment During the Avascular Stage

Next, we evaluate our model and linear predictions against experimental results. Experimental data was obtained using glioblastoma in vitro cultures [25]. Nine sets of measurements were collected from using three levels of glucose (mainly affecting adhesion / bending rigidity) and three levels of bovine serum (mainly affecting proliferation) [25, 14]. Cell clusters were initially grown to tumor spheroids using a liquid-overlay technique [26]. Spheroids were then placed in 48-well plates. A Leitz

microscope with magnification x100 was used to observe spheroid growth for 36 days. Photographs had a magnification of x160 and they were taken using an Olympus camera using a 1130 by 1430 $\mu m$ window [25]. For each of the levels of glucose and serum, glioblastoma cultures were growing up to a steady state, which corresponds to a diffusion-limited steady-state size. Sample photographs are shown in Figure 7.

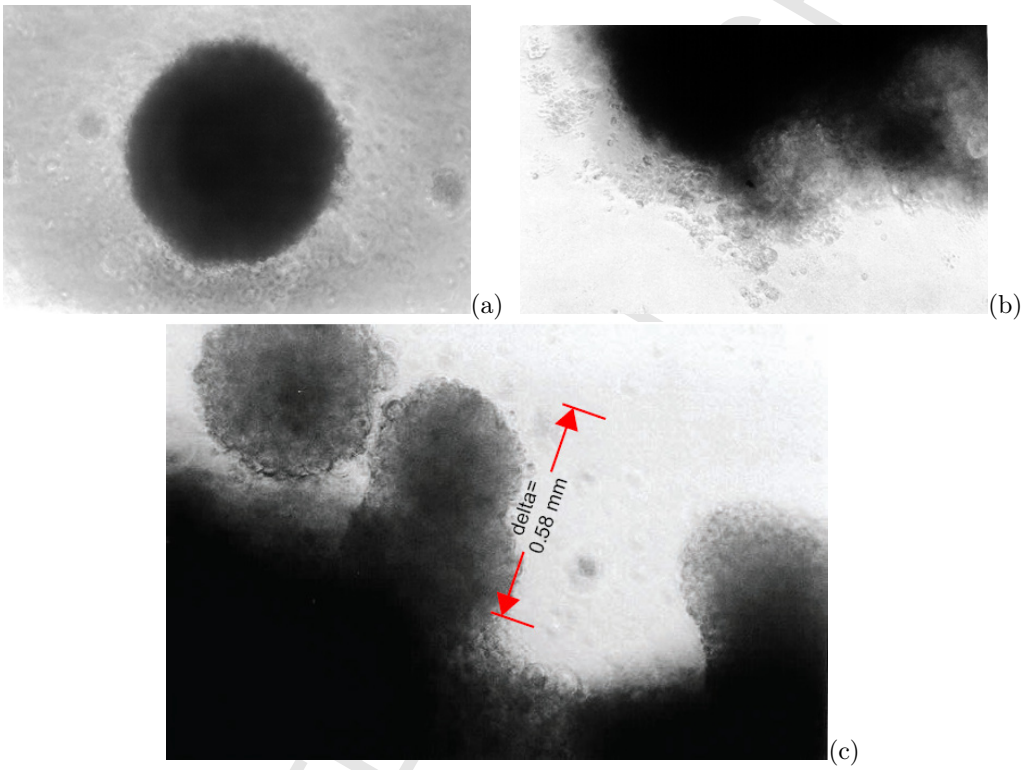


Figure 7: Sample experimental pictures of glioblastoma spheroids [25, 14]. Low Adhesion - High Proliferation (a) and High Adhesion - Low Proliferation (b). Measured protrusion for $l = 3$; high cell adhesion and high proliferation (c) .

We first set $c = 0$ in Eq. (44) and solve for a marginally stable $\mathbb{S}$, which we name $\mathbb{S}_M$ hereafter

$$\mathbb{S}_M = \frac{1}{(3/2 - l^2)}\left[\mathbb{A}\left(1 - \frac{1}{\lambda + 1}\right) + \frac{l}{4R^3} + \frac{1-B}{1+\lambda}\left(1 - \frac{I_1(R)I_{l+1}(R)}{I_0(R)I_l(R)}\right) - (1-B)\frac{2}{R}\frac{I_1(R)}{I_0(R)}\right]. \quad (45)$$

Next, we evaluate our model and linear stability analysis by comparing $\mathbb{S}_M$ with estimated $\mathbb{S}_p$ from the experimental results. The calculation of apoptosis and cell adhesion using a Darcy model had been performed in [25] and [14]. In this work, using our two-phase Stokes model, we estimate $\mathbb{A}$

and $\mathbb{S}$, and use the latter for evaluation against experimental results.

### *6.1. Apoptosis estimates*

Since $\mathbb{A}$ was shown earlier to promote shape instability (see Eq. (44)), we focus on critical $\mathbb{A}$ values obtained from Eq. (43) by setting $\frac{dR}{dt} = 0$. This corresponds to a steady state stage of the in vitro glioblastoma culture [14]. Assuming $\mathbb{B} = 0$, equation (43) reads as

$$\mathbb{A} = \frac{2}{R}\frac{I_1(R)}{I_0(R)}. \tag{46}$$

Note that $R$ is a scaled radius obtained from the experimental results. The experiments presented in [14, 25] suggest that by considering a scaling of $L \approx 125\mu$m [14], the nondimensional spheroid radii range: $6.24 \leqslant R \leqslant 7.528$. Therefore, the corresponding range for the apoptosis parameter, $0.247342 \leqslant \mathbb{A} \leqslant 0.293569$, following Eq. (46).

In Figure 8[a], we take $\lambda = 0.1$ and show the $\mathbb{S}_M$ curves as functions of $R$ for different $l$ values. For each $l$, the curve divides the parameter region into unstable (top right) and stable (bottom left) subregions. The figure suggests that larger $l$ values lead to sharper increases of the $\mathbb{S}_M$ curves for the range of radial values considered in this study (especially for $6.24 \leqslant R \leqslant 7.528$). Figure 8[b] shows how the $\mathbb{S}_M$ curves change with respect to $\lambda$ for a given mode $l = 3$, indicating that a small viscosity ratio gives a large unstable region.

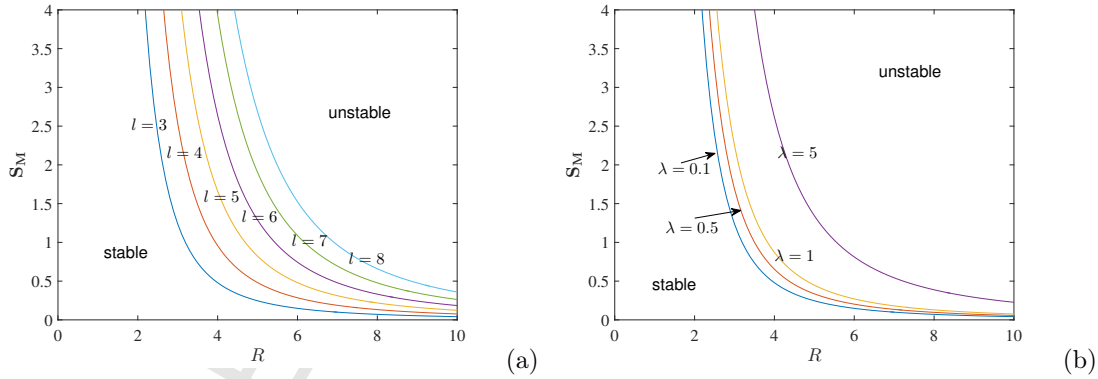


Figure 8: (a) $\mathbb{S}_M$ as a function of $R$, for different $l$ values, here $\lambda = 0.1$. (b) $\mathbb{S}_M$ as a function of $R$, for different $\lambda$ values, here $l = 3$.

*6.2. Bending rigidity estimates*

We approximate $\frac{dR}{dt}$ near $R \approx 0$ and obtain the following net mitosis rate [14]

$$\tilde{\lambda}_M = \frac{1}{2}(1 - \mathbb{A})\lambda_M. \tag{47}$$

Without loss of generality, we focus our study on an interface perturbed by a cosine mode, $\bar{r}(\theta) = \bar{R} + \bar{\delta}\cos(l\theta)$, where $\bar{R} = RL$ and $\bar{\delta} = \delta L$ represent the dimensional tumor radius and perturbation, respectively. The linear form of the bending energy reads as

$$\frac{1}{2}\mathcal{K}^3 + \mathcal{K}_{ss} = \frac{1}{2\bar{R}^3} - \frac{\bar{\delta}(l^2-1)(2l^2-3)}{2\bar{R}^4}\cos(l\theta). \tag{48}$$

Using the Stokes equation and the stress jump condition, we obtain the following characteristic values

$$\bar{T}_- \sim \tilde{\lambda}_M\mu_- + \tilde{\lambda}_M\mu_-\frac{\bar{\delta}}{\bar{R}}\cos(l\theta), \tag{49}$$

$$\bar{T}_- \sim \nu_0\left(\frac{1}{2\bar{R}^3} - \frac{\bar{\delta}(l^2-1)(2l^2-3)}{2\bar{R}^4}\cos(l\theta)\right), \tag{50}$$

where Eq. (49) represents the characteristic stress in the proliferating rim and Eq. (50) represents the characteristic stress from tumor boundary. Dividing by $\tilde{\lambda}_M\mu_-$, we obtain

$$1 + \frac{\bar{\delta}\cos(l\theta)}{\bar{R}} \sim \frac{\nu_0}{\tilde{\lambda}_M\mu_-}\left(\frac{1}{2\bar{R}^3} - \frac{\bar{\delta}(l^2-1)(2l^2-3)}{2\bar{R}^4}\cos(l\theta)\right). \tag{51}$$

Using the definition of $\mathbb{S}^{-1} = \dfrac{\nu_0}{\mu_-\lambda_M L^3}$ and combining with Eq. (47), we obtain the maximum $\mathbb{S}_p$ by taking $\cos(l\theta) = -1$,

$$\mathbb{S}_p = \frac{1}{1-\mathbb{A}}\left(\frac{1}{R^3} + \frac{1 + (l^2-1)(2l^2-3)}{R^4}\delta\right). \tag{52}$$

We next compare the marginally stable $\mathbb{S}_M$ against the predicted $\mathbb{S}_p$ by using the experimental data in [14, 25]. We take $L \approx 125\mu m$ for the spheroid radii [14], and set mode number $l = 3, 4$, and 5. In [25], the authors considered that $\mathbb{A}$ was small and therefore neglected its effects. In this paper, we would like to explore this parameter and consider the minimum apoptosis found in the previous subsection with $\mathbb{A} = 0.247342$. Note that the calculation of Eq. (52) also requires the value of perturbation $\delta$. This can be done by equating the corresponding coefficients from Eqs. (41) and (42) to get $\delta(l = 3) = 0.894403$, $\delta(l = 4) = 0.70909$, and $\delta(l = 5) = 0.590181$.

In Figure 9, we plot the predicted $\mathbb{S}_p$ as a function of the non-dimensional $R$ scaled by $L \approx 125\mu m$, which is denoted by markers. The analytic critical $\mathbb{S}_M$ as a function of $R$ for different

values of $\lambda$ are plotted using colored lines. Here low proliferation is denoted by circles, medium proliferation by stars, and high proliferation by triangles. The high cell adhesion is denoted by blue color, medium cell adhesion by black color, and low cell adhesion by red color. Note that the experimental qualitative values, where index 1 indicates a very stable morphology and index 5 indicates very unstable [14], are listed together with the corresponding markers. For example, the points indicated by index "2" (almost stable), represent the nondimensional steady tumor spheroid radius of $R = 7.528$ and its corresponding predicted $\mathbb{S}_p$.

As shown in Figure 9, for $l = 3$, analytic critical $\mathbb{S}_M$ with smaller $\lambda$ agrees with the predicted $\mathbb{S}_p$ better. As $l$ increases, larger $\lambda$ yields better agreement between $\mathbb{S}_p$ and $\mathbb{S}_M$, e.g. $\lambda = 0.1$ for $l = 4$ and $\lambda = 0.2$ for $l = 5$. For mode values $l = 4$ and $l = 5$, Figure 9 suggests that our model is consistent with the experimental findings for all scenarios except the medium cell bending and medium proliferation. A possible reason for this is that the value of the viscosity ratio $\lambda$ is not always known from experiments, and $\lambda$ can be a value varying from one experiment to another. It's possible that the $\lambda$ value in the experiment for the medium cell bending and medium proliferation case is higher than others, which increases the tumor stability.

## 7. Conclusion

In this paper, we performed a linear stability analysis of a 2D, non-circular tumor with isotropic bending rigidity growing in a host tissue. The interior tumor and exterior host were modeled by the Stokes flow and the tumor host interface was modeled by an elastic membrane governed by the Helfrich bending energy. Using an energy variation approach, we derived a modified Laplace-Young condition for the stress jump across the interface in the Stokes equation. We then investigated how physical parameters such as viscosity, bending rigidity, and apoptosis contribute to the morphological stability of the interface.

The linear analysis shows that an increase in bending rigidity contributes to an increase in tumor's morphological stability, almost independently of changes in other parameters. During avascular growth, it is observed that an increase in the apoptosis leads to an overall increase in shape instabilities. It was also observed that without apoptosis, an increase in vascularization leads to a self-similar growth for large tumor size, almost independently of the viscosity ratio. It should be noted that these results do not necessarily mean that there is a biological causal relationship, and more research, especially experimental studies, need to be done to build such a reliable causal

relationship. Nevertheless, these results are still able to provide potential insight to reduce shape instabilities of certain kinds of tumors.

Our findings are consistent with previously conducted simulations, which reveal that when the tumor is more viscous than its environment, its morphology becomes more unstable and patterns like fingers and branched structure could occur [24, 7, 14]. In addition, comparison with experimental data on glioblastoma spheroids shows good agreement, especially for tumors with high bending and low proliferation. We are currently performing nonlinear simulations to confirm that our 2D model indeed captures the significant features discovered in linear theory. In future work, we will also consider adding a stochastic component to our work and establish a linear stability theory consistent with the newly developed model.

**Acknowledgments.** S. L. and J. L. acknowledge the support from the National Science Foundation, Division of Mathematical Sciences (NSF-DMS) grants DMS- 1719960 (J. L.) and DMS-1720420 (S. L.). S. L. is also partially supported by grant ECCS-1307625. J.L. also acknowledges partial support from NIH grant P50GM76516 for a Center of Excellence in Systems Biology at the University of California, Irvine. S.L. and J.L. also want to thank Dr. H. Frieboes for the experimental data. Special thanks to Dr. Marian Gidea for his precious inputs related to the theoretical aspects of this work. Also, I would like to thank Dr. Julius Turian, Rush University, for helpful comments.

## References

[1] H. Byrne, Using mathematics to study solid tumour growth, in: Proceedings of the 9th General Meetings of European Women in Mathematics, 2000, pp. 81–107.

[2] R. Gatenby, Mathematical models of tumor-host interactions, The Cancer Journal 11 (6) (1998) 289–293.

[3] R. A. Gatenby, P. K. Maini, Mathematical oncology: cancer summed up, Nature 421 (6921) (2003) 321–321.

[4] H. Greenspan, On the growth and stability of cell cultures and solid tumors, Journal of theoretical biology 56 (1) (1976) 229–242.

[5] H. Byrne, M. A. J. Chaplain, Growth of nonnecrotic tumors in the presence and absence of inhibitors, Mathematical biosciences 130 (2) (1995) 151–181.

[6] A. Friedman, F. Reitich, Analysis of a mathematical model for the growth of tumors, Journal of mathematical biology 38 (3) (1999) 262–284.

[7] V. Cristini, J. Lowengrub, Q. Nie, Nonlinear simulation of tumor growth, Journal of mathematical biology 46 (3) (2003) 191–224.

[8] A. Friedman, B. Hu, Bifurcation for a free boundary problem modeling tumor growth by stokes equation, SIAM Journal on Mathematical Analysis 39 (1) (2007) 174–194.

[9] A. Friedman, F. Reitich, Quasistatic motion of a capillary drop i. the two-dimensional case, Journal of Differential Equations 178 (1) (2002) 212–263.

[10] S. Franks, J. King, Interactions between a uniformly proliferating tumour and its surroundings: uniform material properties, Mathematical medicine and biology 20 (1) (2003) 47–89.

[11] J. King, S. Franks, Mathematical analysis of some multi-dimensional tissue-growth models, European Journal of Applied Mathematics 15 (3) (2004) 273–295.

[12] J. King, S. Franks, Mathematical modelling of nutrient-limited tissue growth, in: Free Boundary Problems, Springer, 2006, pp. 273–282.

[13] A. Friedman, B. Hu, Bifurcation from stability to instability for a free boundary problem modeling tumor growth by stokes equation, Journal of mathematical analysis and applications 327 (1) (2007) 643–664.

[14] K. Pham, H. B. Frieboes, V. Cristini, J. Lowengrub, Predictions of tumour morphological stability and evaluation against experimental observations, Journal of The Royal Society Interface (2010) rsif20100194.

[15] S. K. Bhatia, Engineering biomaterials for regenerative medicine: novel technologies for clinical applications, Springer Science & Business Media, 2011.

[16] M. Denis, A. Gregory, M. Bayat, R. T. Fazzio, D. H. Whaley, K. Ghosh, S. Shah, M. Fatemi, A. Alizad, Correlating tumor stiffness with immunohistochemical subtypes of breast cancers:

Prognostic value of comb-push ultrasound shear elastography for differentiating luminal subtypes, PloS one 11 (10) (2016) e0165003.

[17] J. Fenner, A. C. Stacer, F. Winterroth, T. D. Johnson, K. E. Luker, G. D. Luker, Macroscopic stiffness of breast tumors predicts metastasis, Scientific reports 4.

[18] S. E. Reid, E. J. Kay, L. J. Neilson, A.-T. Henze, J. Serneels, E. J. McGhee, S. Dhayade, C. Nixon, J. B. Mackey, A. Santi, et al., Tumor matrix stiffness promotes metastatic cancer cell interaction with the endothelium, The EMBO journal 36 (16) (2017) 2373–2389.

[19] A. He, J. Lowengrub, A. Belmonte, Modeling an elastic fingering instability in a reactive hele-shaw flow, SIAM Journal on Applied Mathematics 72 (3) (2012) 842–856.

[20] Y. Sui, Y. Chew, P. Roy, X. Chen, H. Low, Transient deformation of elastic capsules in shear flow: effect of membrane bending stiffness, Physical Review E 75 (6) (2007) 066301.

[21] A. Tian, B. R. Capraro, C. Esposito, T. Baumgart, Bending stiffness depends on curvature of ternary lipid mixture tubular membranes, Biophysical journal 97 (6) (2009) 1636–1646.

[22] H. Shiba, H. Noguchi, Estimation of the bending rigidity and spontaneous curvature of fluid membranes in simulations, Physical Review E 84 (3) (2011) 031926.

[23] I. Urrutia, Bending rigidity and higher-order curvature terms for the hard-sphere fluid near a curved wall, Physical Review E 89 (3) (2014) 032122.

[24] K. Pham, E. Turian, K. Liu, S. Li, J. Lowengrub, Nonlinear studies of tumor morphological stability using a two-fluid flow model, Journal of Mathematical Biology (2018) https://doi.org/10.1007/s00285–018–1212–3.

[25] H. B. Frieboes, X. Zheng, C.-H. Sun, B. Tromberg, R. Gatenby, V. Cristini, An integrated computational/experimental model of tumor invasion, Cancer research 66 (3) (2006) 1597–1604.

[26] R. Sutherland, J. Carlsson, R. Durand, J. Yuhas, Spheroids in cancer research, Cancer research 41 (7) (1981) 2980–2984.

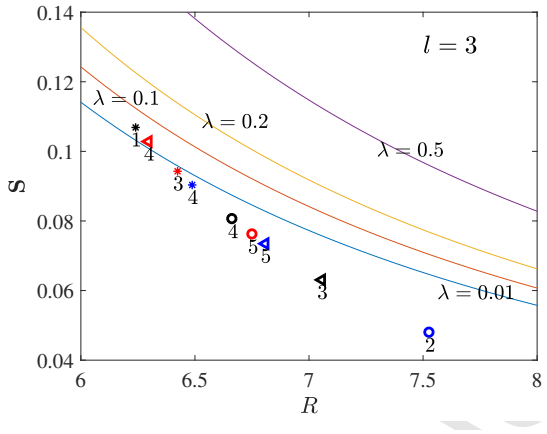


(a)

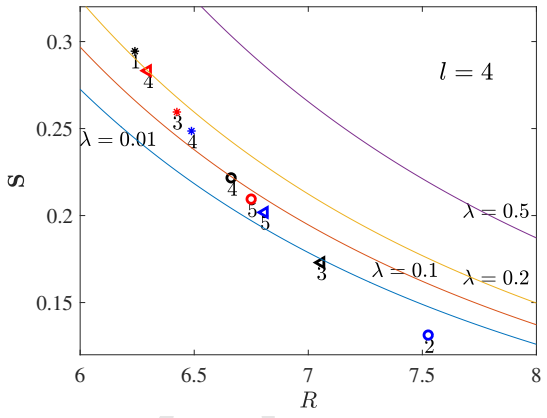


(b)

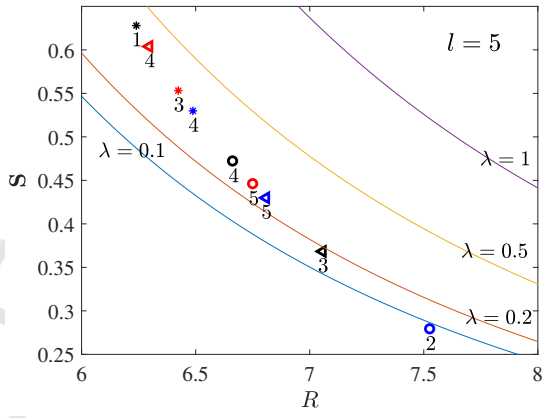


(c)

Figure 9: $\mathbb{S}_M$ as a function of $R$, for $l = 3$(a), $l = 4$(b), and $l = 5$(c). $S_p$ points represented by their qualitative numbers. Here low proliferation is denoted by circles, medium proliferation by stars, and high proliferation by triangles. The high bending is denoted by blue color, medium cell bending by black color, and low cell bending by red color.